International Journal of Greenhouse Gas Control 41 (2015) 1–10

Contents lists available at ScienceDirect

International Journal of Greenhouse Gas Control

journal homepage: www.elsevier.com/locate/ijggc

A theoretical study of the reaction kinetics of amines released into the atmosphere from CO_2 capture

Saba Manzoor[a], Alexandra Simperler[b], Anna Korre[a,*]

[a] Department of Earth Science and Engineering, Royal School of Mines, Imperial College London, London SW7 2BP, UK
[b] Department of Chemistry, Imperial College London, SW7 2AZ, UK

ARTICLE INFO

Article history:
Received 25 November 2014
Accepted 11 May 2015

Keywords:
Post combustion CO_2 capture
Monoethanol amine
Nitrosamine
Nitramine
Atmospheric chemistry modelling
Atmospheric dispersion

ABSTRACT

Amine solvents used in CO_2 capture technologies result in the release of compounds such as nitrosamines and nitramines to the atmosphere. The reaction kinetics of monoethanolamine and the resulting degradation amines, methylamine and dimethylamine, are studied using transition state and collision theory. A simplified amine atmospheric chemistry scheme and three types of reactions,—with barrier, without a barrier and a photolysis reaction—are considered using geometric, energetic and thermodynamic data derived from quantum chemistry and kinetic modelling. The rate coefficients obtained are in excellent agreement with existing experimental and theoretical values. These coefficients are used within the Amine Chemistry Module of the atmospheric dispersion model ADMS 5 to solve the advection-dispersion-chemical equations. A case study on the Technology Centre Mongstad is conducted to estimate the dispersion, chemical transformation and transport pathways of these amines away from the emitting facility. Reliable estimates of the concentrations of the resulting nitrosamines and nitramines are determined and compared to safety guideline values to establish the risk these discharges may pose on the environment. This study illustrates the theoretical methodology developed and its implementation within the ADMS 5 atmospheric dispersion model, which can be used at any amine based CO_2 capture facility regardless of its geographical location.

1. Introduction

The post combustion power generation technology, using amines as solvent for CO_2 capture, is one of the technologies employed to combat the escalating CO_2 levels in the atmosphere. An amine-based monoethanolamine solvent (MEA) is considered the reference solvent for post combustion CO_2 capture (PCCC), due to its fine adsorption–desorption properties towards CO_2 (Bråten et al., 2009). Despite the efforts to clean the flue gas, small amounts of amine degradation products get entrained in the flue gas during the capture process and form part of the emissions into the atmosphere. The degradation products, nitrosamines (NS) and nitramines (NA), are suspected carcinogens in mammals at extremely low concentrations (Karl et al., 2008; Låg et al., 2011; Reh et al., 2000). It is therefore essential to determine the fate of these compounds in the atmosphere by studying their chemical transformation, dispersion and transport. The chemical transformation requires studying the mechanisms and kinetics of the reactions involved. Thereof, deduced rate constants may serve as input variables for advection-diffusion-reaction equations to determine accurately the levels of these chemical discharges in the air. The obtained concentration estimates of individual species can be used to assess the health risk they pose.

In this study, the three most likely amines and nitrosamine that form as a consequence of volatilization of the emissions are investigated. These consist of MEA and the potential degradation products formed during the amine scrubbing process; namely, methylamine (MA), dimethyl amine (DMA) and nitroso dimethylamine (NDMA).

Following the emission of the amines and amine degradation products into the atmosphere, they undergo various reactions (Table 1). OH radicals, which are abundant in the atmosphere as they are naturally produced from the photolysis of O_3, can abstract a hydrogen atom from the NH_2 group of an amine to form an amino radical. This highly unstable and very reactive radical species undergoes additional reactions with NO and NO_2 to form nitrosamines (or alkyldiazohydroxides in the case of primary nitrosamines) and nitramines, which are harmful to both humans and the natural environment (Knudsen et al., 2009). The amino

* Corresponding author.
E-mail address: a.korre@imperial.ac.uk (A. Korre).

http://dx.doi.org/10.1016/j.ijggc.2015.05.012
1750-5836/

Table 1
Reaction scheme and the corresponding rate constants of Monomethylamine (MA), dimethylamine (DMA) and monoethanolamine (MEA).

MA					
$CH_3NH_2 + OH$	→	$CH_3NH + H_2O$			k_1
	→	$CH_2NH_2 + H_2O$			k_{1b}
$CH_3NH + O_2$	→	$CH_2{=}NH_2 + O_2H$			k_2
$CH_3NH + NO$	→	$CH_3NH{-}NO$			k_3
			hυ →	$CH_3NH + NO$	J_5
$CH_3NH + NO_2$	→	$CH_3NH{-}NO_2$	→	$CH_2{=}NH_2 + HONO$	k_{4a}
					k_{4b}
DMA					
$(CH_3)_2NH + OH$	→	$(CH_3)_2N + H_2O$			k_1
	→	$(CH_3)NHCH_2 + H_2O$			k_{1b}
$(CH_3)_2N + O_2$	→	$CH_2{=}N{-}CH_3 + O_2H$			k_2
$(CH_3)_2N + NO$	→	$(CH3)_2N{-}NO$			k_3
			hυ →	$(CH_3)_2N + NO$	J_5
$(CH_3)_2N + NO_2$	→	$(CH_3)_2N{-}NO_2$			k_{4a}
			→	$CH_2{=}N{-}CH_3 + HONO$	k_{4b}
MEA					
$OH(CH_2)_2NH_2 + OH$	→	$OH(CH_2)_2NH + H_2O$			k_1
	→	$OHCH_2CHNH_2 + H_2O$			k_{1b}
	→	$OHCHCH_2NH_2 + H_2O$			k_{1c}
	→	$O{-}(CH_2)_2NH_2 + H_2O$			k_{1d}
$OH(CH_2)_2NH + O_2$	→	$OHCH_2CH{=}NH + O_2H$			k_2
$OH(CH_2)_2NH + {}^{\bullet}NO$	→	$OH(CH_2)_2NH{-}NO$			k_3
			hυ →	$OH(CH_2)_2NH + NO$	J_5
$OH(CH_2)_2NH + NO_2$	→	$OH(CH_2)_2NH{-}NO_2$			k_{4a}
			→	$HOCH_2CH{=}NH + HONO$	k_{4b}

radical also reacts with O_2 to form the corresponding imine, which is non-toxic. An imine can also be formed from the nitrosamine and nitramines. In sunlight, the nitrosamine undergoes photolysis reactions to form an amino radical, which can once again react with the mentioned radicals to repeat the whole cycle of reactions.

The atmospheric chemistry of the amines is complex and, due to their high vapour pressures at atmospheric conditions, performing experimental investigations resembling realistic conditions is challenging. Nevertheless, a few experimental investigations on amine degradation have been carried out in the laboratory. A few of these studies focus on the determination of the rate constant for the reactions of amines with ·OH radicals (Anderson and Stephens, 1988; Atkinson et al., 1977; Carl and Crowley, 1998; GORSE et al., 1977; Harris and Pitts, 1983; Karl et al., 2012; Koch et al., 1996; Nielsen et al., 2012; Onel et al., 2012 Harris and Pitts, 1983; Karl et al., 2012; Koch et al., 1996; Nielsen et al., 2012; Onel et al., 2012). A few others have investigated the gas phase reactions of alkyl amino radicals with NO, NO_2, O_2 (Lazarou et al., 1994; Lindley et al., 1979; Nielsen et al., 2011a; Tuazon et al., 1994, 1984). Some pilot plant studies have been conducted to characterise the amine degradation products (Lepaumier et al., 2011; Strazisar et al., 2003).

As the experimental investigations are relatively sparse, quantum chemistry calculations may be an option to fill the gaps in available literature. Some have been performed to determine the rate of reaction of alkylamine with OH radicals (Galano and Alvarez-Idaboy, 2008; Onel et al., 2013; Tian et al., 2009). Recently, scientists have determined rates for MEA and •OH reactions (Nielsen et al., 2011b; Onel et al., 2012; Xie et al., 2014). However, due to the limited number of studies performed both at experimental and theoretical levels; the atmospheric chemistry of the amines has not been fully explored.

The released amine emissions disperse in the atmosphere and their concentration is a function of distance from the source as well as their chemical fate. Dispersion calculations combined with atmospheric chemistry assist in quantifying this effect. Previous studies have assumed experimentally determined fixed formation yields to account for the NA and NS concentrations (de Koeijer et al., 2013; Karl et al., 2011). In their studies, only the atmospheric dispersion of MEA was considered and the concentration of the NS and NA is represented as a fraction of this with distance from the source, which is a coarse approximation. Another limitation of this approach is its dependency on experimental values, which are sparse.

In this study, to establish for a more accurate methodology, rate constants describing the atmospheric chemistry scheme for each of the amines considered are calculated using quantum chemistry and kinetic modelling. These tools are capable of estimating gas-phase reaction kinetics within experimental accuracy (Galano et al., 2006) and are applicable to all amines. The rate constants assist in gaining a better understanding of actual concentrations of the product species over time and space. As the methodology proposed here is independent from experimental conditions, it may be universally applicable in establishing a better understanding of the atmospheric chemistry of amine emissions from PCCC.

In order to investigate the chemical transformation of amines emitted from a capture plant together with their dispersion and transport, the specially designed Amine Chemistry Module in the ADMS 5 atmospheric dispersion model (CERC, 2012a,b) is employed. Within ADMS 5, it is possible to describe the entire atmospheric fate of the involved amines, including their growth and decay as previously reported by CERC (CERC, 2012c,d).

The reaction scheme employed in the work described here is presented in Table 1 and covers Monomethylamine (MA), dimethylamine (DMA) and monoethanolamine (MEA).

The system of ordinary differential equations used to solve this atmospheric chemistry scheme in ADMS 5 is summarised in Table 2 and is implemented using the newly determined rate constants. The world's largest facility for testing and improving technologies for CO_2 capture and storage technology, Technology Centre Mongstad (TCM) is considered as the emitting source to illustrate the implementation. TCM can capture 100,000 tonnes of CO_2 per year with a CO_2 capture rate of 85%. The likely case of amine emissions from the facility used in this study is taken from CERC (2012d). The amine and amine degradation product concentrations estimated using the methodology developed are

Table 2
The differential equations used in ADMS 5 to solve the atmospheric chemistry scheme (after CERC, 2012c).

Loss of the amine	$\frac{d[\text{Amine}]}{dt} = -k_1[\text{OH}][\text{Amine}]$
Production of the amino radical	$\frac{d[\text{Radical}]}{dt} = k_1[\text{OH}][\text{Amine}] + J_5 h\upsilon[\text{Nitrosamine}] - k_2[\text{Radical}][\text{O}_2] - k_3[\text{Radical}][\text{NO}] - k_{4a}[\text{Radical}][\text{NO}_2]$
Production of nitrosamine	$\frac{d[\text{Nitrosamine}]}{dt} = k_3[\text{Radical}][\text{NO}] - J_5 h\upsilon[\text{Nitrosamine}]$
Production of nitramine	$\frac{d[\text{Nitramine}]}{dt} = k_{4a}[\text{Radical}][\text{NO}_2] - k_{4b}[\text{Nitramine}]$

compared to the safety guideline values established by Norwegian Institute for Air Research (Knudsen et al., 2009) to perform a risk assessment.

2. Atmospheric chemistry computational details

2.1. Atmospheric chemistry model

All quantum chemical calculations have been performed with the Gaussian 09 model for electronic structure (Frisch et al., 2009). In order to estimate the barrier height of the reaction from reactants to products via a transition state, an error of 1 kcal/mol was allowed. For the purposes of this work a range of functional and basis sets were tested (see Table S1, supplementary materials). The M062X functional (Fernandez-Ramos et al., 2006; Zhao and Truhlar, 2008; Zheng et al., 2009) and the 6-31 *G* (2d, p) basis set (Pople et al., 1987) produced reaction rates closest to experiment (i.e. k_{OH} for MA), which made them a suitable choice. The geometry optimisations of all the stationary points on the potential energy surface (PES) of the target amines and their reaction partners were calculated using the above level of theory. Stationary points such as minima and transition states on the minimum energy path of these PESs were characterised with frequency calculations.Three distinct types of reactions were considered: (i) reactions with a barrier, (ii) reactions without a barrier and (iii) a photolysis reaction. Transition state theory (TST) and Rice-Ramsperger-Kassel-Marcus (RRKM) theory were applied to determine the rate constants of interest.

2.2. Reactions described with transition state theory

Transition states were located with the QST2 method (Peng et al., 1996; Peng and Bernhard Schlegel, 1993) by starting from the reactant and product geometries. For the radical reactions, the starting point chosen was a geometry that was a maximum energy in a PES scan along the reaction coordinate. This estimated transition state was then optimised towards a saddle point of the first order. Then intrinsic reaction coordinate (IRC) calculations were performed to find the corresponding reactants and products. To calculate the rate for the reaction between the amine and the OH radical, ΔG was determined as the difference between the free energy of the reactant and the transition state. ΔG is then used in Eyring–Polanyi's Eq. (1) (Eyring, 1935) to calculate the rate constant, k_1, which accounts for the rate of formation of the alkyl amino radical and H_2O. The Wigner tunnelling correction factor (Γ) (Eq. 2) (Wigner, 1932) is used for correcting the rate constant.

$$k(T) = \Gamma(T)\frac{k_B T}{h} e^{\left(-\frac{\Delta G^{\neq}}{RT}\right)} \quad (1)$$

$$\Gamma(T) = 1 + \left(\frac{1}{24}\right)\left(\frac{|\upsilon^{\neq}|}{k_B T}\right)^2 \quad (2)$$

Where $\Delta G^{\neq}$ is the Gibbs energy of activation, k_B is Boltzmann's constant, $\hbar$ is Planck's constant, T is absolute temperature and $\upsilon^{\neq}$ is the imaginary frequency of the asymmetric stretch along the reaction coordinate. k_1 values for the amines + OH reactions were also determined by using EPI-Suite (Atkinson et al., 1977) which is a structure-activity-relationship (SAR) programme developed by the EPA's Office of Pollution Prevention Toxics and Syracuse Research Corporation (SRC).

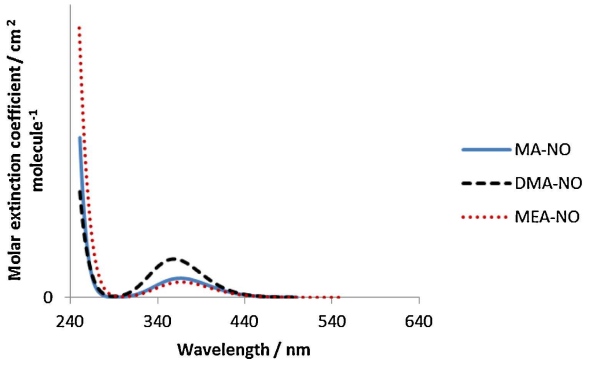

Fig. 1. TD-DFT (B3LYP/ aug-ccpTVZ) predictions of the total molar extinction coefficient (cm^2 $molecule^{-1}$) versus wavelength for the three nitrosamines of interest in the spectral region for tropospheric photolysis.

2.3. Reactions described with RRKM theory

For the alkyl amino radicals and NO and NO_2 barrierless radical recombination reactions (k_3 and k_{4a} in Table 1), the calculations of high-pressure rate constants and thermal functions were performed with ChemRate 1.5.8 (Mokrushin et al., 2011) at 298.15 K and 1 atm. ChemRate contains a master equation solver that determines the rate constants for the reactions in the energy transfer region under non-steady state conditions using RRKM theory (Barker and Golden, 2003). This is based on density and sum of states for the M062X optimised geometries. Argon was used as bath gas considered for the calculations. The collisional energy transfer was described using an exponential-down model. The Lennard Jones parameters for the active species have been obtained using their experimental critical temperature and the critical pressure (Thermopedia™, 2014) of their non-radical species in case of a radical. ChemRate was also used for calculating k_2 and k_{4b} (Table 1).

2.4. Photolysis

To determine the rate of the nitrosamine photolysis [J_5 $h\upsilon$ pathway in Table 1], time-dependent density functional theory, TD-DFT, (Kootstra et al., 2000; Romaniello and de Boeij, 2005), using the B3LYP (Becke, 1988; Stephens et al., 1994) hybrid functional and the aug-ccpVTZ basis set (Dunning, 1989), was employed to calculate the UV–vis spectra (Fig. 1) of the nitrosamines. Prior to the TD-DFT calculations, geometries of the studied nitrosamines were optimised using the same level of theory. TD-DFT (B3LYP/aug-ccpTVZ) gave a more accurate determination of the vertical excitation wavelength and oscillator strength (see Table S2, Supplementary materials) than M062X/6-31G (2d,p) and is very useful in estimating accurate UV–vis absorption spectra for medium sized organic substances (Silva-Junior et al., 2008).

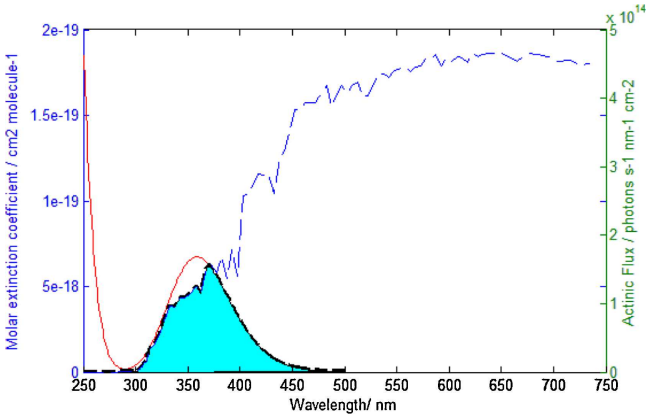

Fig. 2. The overlap region of the simulated UV–vis absorption spectrum of N-nitroso dimethylamine (TD-DFT / B3LYP/aug-ccpVTZ) and the solar actinic flux curve for mid-day 21st June 2012 at TCM.

Lifetimes (τ) are estimated by calculating the photolysis rate constant (J_5 $h\upsilon$). This is determined by numerically integrating the intersection area between the simulated UV spectrum and solar actinic flux at a particular geographical location and time of the year in the region of the $n \rightarrow \pi^*$ electronic transition centred around 365 nm, as follows:

$$J = \int F(\lambda)\sigma(\lambda, T)\Phi(\lambda, T)d\lambda \quad (3)$$

$$\tau_{\text{Photolysis}} = \frac{1}{J} \quad (4)$$

where J is the photolysis rate (J_5 $h\upsilon$) which is a function of $F(\lambda)$, the solar actinic flux at a specified latitude, longitude and time of the year (photons s^{-1} nm^{-1} cm^{-2}), $\sigma(\lambda,T)$ is the molar extinction coefficient (cm^2 $molecule^{-1}$) at the wavelength and temperature of the chemical substance and $\Phi(\lambda,T)$ is the quantum yield of the photolysis reaction (value of 1). The photolysis frequency, τ, expresses the rate of photolysis as a first-order decay process and, therefore, the reciprocal of this value gives the nitrosamine photolysis lifetime.

Fig. 2 illustrates the overlap region of the simulated UV–vis absorption spectrum of N-nitroso dimethylamine and the solar actinic flux curve generated using the Tropospheric Ultraviolet and Visible (TUV) Radiation Model from the National Centre for Atmospheric Research (NCAR) for the TCM latitude and longitude on 21st June 2012 and at 65 m stack height.

3. Results and discussion

3.1. Calculated rate constants of the three amines of interest

As already discussed, most of the previous work determined the rate constant for the reactions of amines with OH radicals (Anderson and Stephens, 1988; Atkinson et al., 1977; Carl and Crowley, 1998; Gorse et al., 1977; Harris and Pitts, 1983; Karl et al., 2012; Koch et al., 1996; Nielsen et al., 2012; Onel et al., 2012). Only a few scientists have investigated the gas phase reactions of alkyl amino radicals with NO, NO_2, O_2 or the reactions of dimethyl amino radicals (Lazarou et al., 1994; Lindley et al., 1979). Lindley experimentally determined the relative rates of $k_2/k_3 = (1.48 + 0.07) \times 10^{-6}$, $k_2/k_{4a} = (3.90 + 0.28) \times 10^{-7}$, and $k_{4b}/k_{4a} = 0.22 + 0.06$. The following sections describe the derivation of reaction rates of the complete reaction scheme and Table 3 lists the calculated rate constants. As shown in Table 3, the calculated rate coefficients for DMA are in very good agreement (i.e. within the same order of magnitude) to those determined experimentally. It is therefore assumed that the level of theory used for DMA is appropriate for MA and MEA. The k_1 rate closely agrees to those calculated using EPI-Suite except for MEA. The SAR model used by the EPI-Suite is unable to consider the most stable configurations of the amine and the OH radical when estimating the exact barrier height of the reaction and hence cannot predict the exact OH branching ratio (Nielsen et al., 2012). The SAR model does not function well for amines comprising OH groups or bulky amines (Nielsen et al., 2012) and cannot perform an accurate prediction of the rate of reaction of the OH radical with the MEA. The magnitude of the rate constants suggests that the fastest reaction is the reaction of the amine with the OH radical, k_1. The reaction of the amino radical with the O_2 is the slowest. The rate coefficients, k_2, for the amino radicals with O_2 radicals are several orders of magnitude smaller than for the corresponding reactions with NO (k_3) and NO_2 (k_{4a} and k_{4b}) (Tang and Nielsen, 2012). The k_2 values determined using both theories show similar trends and they closely agree to the experimental value for DMA. However, the value determined using TST is an order of magnitude lower and that from RRKM is higher than the experimental value. TST theory considers only thermal equilibrium, whereas RRKM also accounts for pressure which can affect the reaction. Therefore, the values obtained through RRKM are used in this study as they are more reliable.

In the following sections the reaction paths that are essential to obtaining the rate coefficients are discussed in detail using MEA.

Table 3
Rate constants (cm^2 $molecule^{-1}$ s^{-1}) along with the branching ratio for the OH attack calculated at 298K. The nitrosamine photolysis rate constant is reported as ratio of the photolysis rate constant of NO2 (J/J(NO2)).

	k_{OH}	Branching ratio, k_1/k_{OH}	k_2		k_3	k_{4a}	k_{4b}	$J/J(NO_2)$
			RRKM	TST				
MA	2.18×10^{-11}	0.35	3.64×10^{-18}	1.89×10^{-20}	1.70×10^{-12}	9.7×10^{-13}	2.02×10^{-13}	0.53
Exp	2.22×10^{-11}[a]	0.25[b]						
EPI-Suite	2.22×10^{-11}							
DMA	6.26×10^{-11}	0.38	3.64×10^{-18}	3.68×10^{-20}	8.37×10^{-14}	3.15×10^{-13}	1.10×10^{-14}	1.24
Exp	6.49×10^{-11}[c]	0.37[d]	1.24×10^{-19}[d]		8.53×10^{-14}[e]	3.18×10^{-13}[e]	1.0×10^{-14}[d]	0.53[d]
EPI-Suite	6.55×10^{-11}							
MEA	9.20×10^{-11}	0.05	2.49×10^{-16}	3.86×10^{-18}	5.62×10^{-14}	8.40×10^{-15}	4.14×10^{-15}	0.58
Exp	9.31×10^{-11}[f]	0.08[b]						
EPI-Suite	3.58×10^{-11}							

N.B The experimental K_2 and K_{4b} for the DMA are the calculated rates from the ratios reported by Lindley et al., 1979.

[a] Atkinson et al., 1977.
[b] Nielsen et al., 2011.
[c] Carl and Crowley (1998).
[d] Lindley et al., 1979.
[e] Lazarou et al., 1994.
[f] Karl et al., 2012.

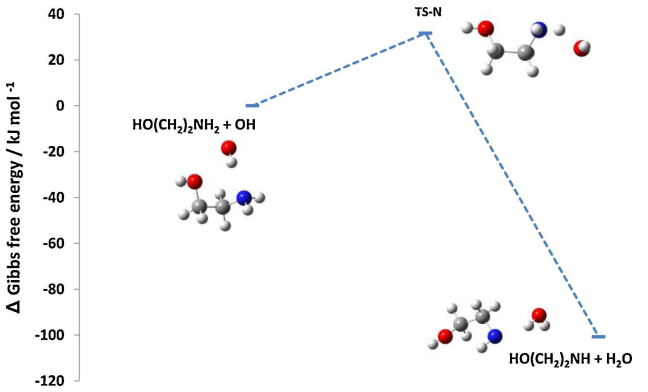

Fig. 3. Energy level diagram for the $HOCH_2CH_2NH_2$ + OH reaction (N-Branch) using M062X/6-31G(2d,p) data.

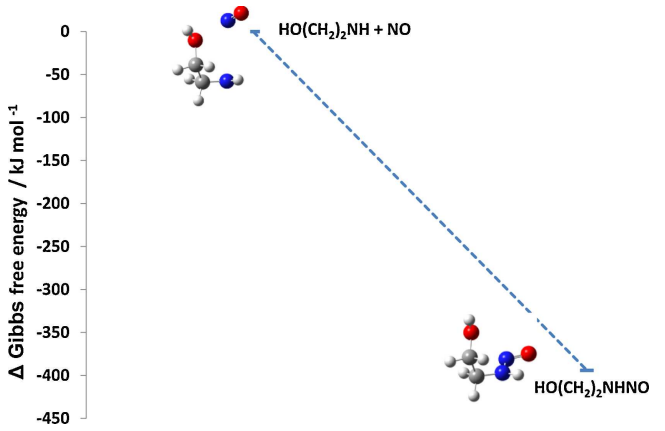

Fig. 4. Energy diagram for $HOCH_2CH_2NH$ + NO reaction using M062X/6-31G(2d,p) data.

Data for DMA and MA are available in the supplementary material (see Figs. S1-7, supplementary materials).

3.2. *Amine + OH reactions* (k_1 *OHpathway)*

When the amine emissions are released into the atmosphere from the PCCC plant they are confronted with abundant as OH radicals. Those can abstract a H atom from either the N of the amino group or the C of the alkyl group, resulting in different proportions of the alkyl amino and alkyl radicals. The alkyl amino radical is of interest as it undergoes further reactions with NO, NO_2 and O_2 forming in particular the harmful nitrosamine and nitramines, as opposed to the alkyl radicals which form aldehydes (Nielsen et al., 2011a). The reactions of the alkyl amino radicals differ from those of the C-centered radicals owing to the difference in their electro-negativities (Tang and Nielsen, 2012).

Before the reaction, the oxygen of the OH radical aligns collinear to the amino N—H and the OH radical forms a H—bond to the N lone pair. During the reaction, the hydrogen leaves the nitrogen atom and joins the OH radical to form the alkyl amino radical and H_2O as the products. The OH group can also align to the C—H of the alkyl group, abstract a hydrogen atom and then form imine and H_2O. Fig. 3 illustrates the reaction starting from a pre-reaction complex and finishing in a post-reaction complex. The transition state structures found are qualitatively geometrically similar to those by (Onel et al., 2012).

As the calculated k_{OH} is supposed to be the sum of rates for H abstraction from an amine group (k_1) and from the non-amine group (k_{1b}) it is essential to consider the following branching ratio:

$$k_{OH} = k_1 + k_{1b} \quad (5)$$

$$\text{OH branching ratio(289K)} = \frac{k_1}{(k_1 + k_{1b})} = \frac{k_1}{k_{OH}} \quad (6)$$

The branching ratio represents the balance between the initial attack on the amino group compared to an attack at the non-amine group. A low branching ratio means fewer amounts of NS and NA are formed. The calculated branching ratios are given in Table 3. The calculated branching ratio for MA + OH is 65C:35N, whereas the experimental branching ratio is found to be 75C:25N (Nielsen et al., 2011a). For DMA + OH, the calculated value is 62C:38N which is very close to the experimental value of 63C:37N. Finally, with MEA + OH, only 5% of the H abstraction occurs at the N, whereas the remaining 95% occurs at both the C and O. The calculated value is lower than the 8% determined by Nielsen et al. (2011a), most likely owing to the variability in the experimental conditions whilst performing the rate determination.

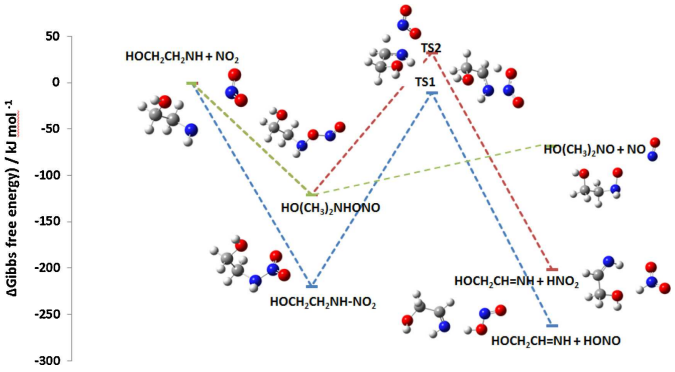

Fig. 5. Energy level diagram for $HOCH_2CH_2NH$ + NO_2 reaction using M062X/6-31G(2d,p) data.

3.3. *Alkyl amino radical reaction + •NO reactions* (k_3 *NO• pathway)*

The reactions of alkyl amines with NO radicals have been the centre of attention due to the production of carcinogenic nitrosamines in the atmosphere (Magee and Barnes, 1956). Generally, secondary alkyl amine radicals, such as the DMA radical, form stable nitrosamines in an exothermic barrierless reaction, which do not undergo further dissociation. Also, MEA forms a stable nitrosamine via a barrierless reaction that does not undergo further dissociation (Fig. 4). This is not the case for MA. Here, primary nitrosamines are formed that are unstable and follow different dissociation pathways to form stable products such as diazomethane (da Silva, 2013). As the likelihood of diazomethane forming is experimentally not supported, the pathway forming the imines, which has been reported experimentally (Nielsen et al., 2011a), is considered.

RRKM theory was employed and the rate constant calculated for the dimethyl amino radical and NO radical (Table 3), which is found to be in excellent agreement to that determined experimentally. There are no reported experimental rate constants for the reaction of methyl amino and monoethanol amino radicals with NO radicals.

3.4. *Alkyl amino radical + NO_2• reactions* ($k_{4a,b}$ *NO_2pathways)*

The alkyl amino radicals are susceptible to attack by NO_2 radicals and can undergo an addition reaction. These reactions are not only exothermic but barrierless, too. A scan of the PES following the reaction coordinate of the N—NO_2 bond cleavage process confirmed

this (Fig. S5, Supplementary materials). In this study, the reaction of the three alkyl amino radicals and NO_2 is investigated considering all the pathways for the proposed products (Fig. 5). This reaction step produces intermediates such as nitramines ($CH_3NH{-}NO_2$, $(CH_3)_2N{-}NO_2$ and $HOCH_2CH_2NH{-}NO_2$) and nitrosoxy amines ($CH_3NH{-}NO_2$, $(CH_3)_2N{-}NO_2$ and $HOCH_2CH_2NH{-}NO_2$). Quantum chemistry calculations have elucidated three dissociation routes for the resulting intermediates which agree to the findings reported by Tang and Nielsen (2012). The N-nitramine dissociates by undergoing a sigmatropic 1,4- H-shift from the adjacent methyl group to the O in the $N{-}NO_2$ via a five-membered-ring transition state, TS1 (Fig. 5). Simultaneously, the N—N bond breaks to form an imine and nitrous acid, HONO. Lindley et al. (1979) have experimentally determined the nitramine/imine branching ratio (0.22 ± 0.06) in the DMA and NO_2 reaction.

The nitrosoxy amine adduct dissociates via two possible routes: (a) a barrierless and an exothermic O—NO bond cleavage process to form an alkyl nitroxide and NO radical (established by performing a bond-fission scan) or (b) a sigmatropic 1,4H-shift from the adjacent methyl group to the N in the O—NO via a five-membered-ring transition state, TS2, forming an imine and nitryl hydride (HNO_2). The later route is likely insignificant in the atmosphere given the high energy of the TS2 relative to TS1 (42.4 kJ/mol).

The determined reaction mechanisms for DMA using quantum theoretical calculations agree well with those from the experiments carried out at atmospheric conditions (Lindley et al., 1979; Nielsen et al., 2011a; Tuazon et al., 1994; Tuazon et al., 1984) in which the production of thermally stable nitramines, N-nitrosoxy amine, imines and HONO or nitroxide and NO radicals were discovered. Theoretical calculations performed by Tang and Nielsen, 2012 support the mechanisms established here for MA and DMA as well.

For the rate constant calculations the rate of reaction of the amino radical with the NO_2 to form NA (k_{4a}) via a barrierless reaction is determined using ChemRate. After the collision between the NO_2 and amino radical to form the NA, the thermally excited NA can then either be quenched by collision or dissociate via TS1 into an imine. The ratio of the imine to the NA is pressure dependent despite a high barrier height (251.3 kJ/mol). The energies of the resulting imine and the NA are comparable (difference of 42.2 kJ/mol) which means that the reaction is in non-equilibrium. Since TST assumes thermal equilibrium RRKM is chosen to calculate k_{4b}.

3.5. *Alkyl amino radical + O_2 reactions (k_2 O_2 pathway)*

Alkyl amino radicals can also undergo H-abstraction reactions with O_2 resulting in imine formation. According to the level of theory employed, the addition of the O_2 to the alkyl amino radical is an exothermic process which proceeds via a transition state to form the peroxy adduct, suggesting that this PES possesses a transition state as shown in Fig. 6 (established by a scan of the bond breaking process, Fig. S7, supplementary materials). These findings are not in agreement to those from Tang and Nielsen, 2012, where it was suggested that such a reaction is barrierless. However, the three dissociation routes for the resulting intermediates calculated, agree to the findings reported by these authors (Tang and Nielsen, 2012). The peroxy adduct dissociates via two possible pathways to give a H—bonded imine and hydroperoxyl (HO_2) product complex. The first occurs via a sigmatropic 1,4H-shift from the adjacent methyl group to the O atom in the OON plane via a five-membered-ring transition state, TS2, breaking the N—O bond and forming the C=N bond simultaneously. The second one occurs via a sigmatropic 1,4H-shift from the adjacent methyl group to the O atom via a four-membered-ring transition state, TS4 (with an O—H bond). The barrier height of TS2 is lower by 118.4 kJ/mol than that of TS4 owing to differences in their geometries.

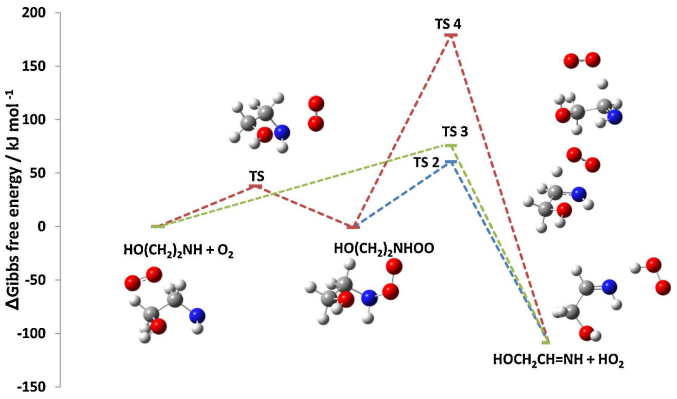

Fig. 6. Energy level diagram for $HOCH_2CH_2NH + O_2$ reaction using M062X/6-31G(2d,p) data.

The imine and HO_2 product complex is also formed by abstracting a H atom directly from the alkyl amino radical proceeding via transition state, TS3. However, owing to the relatively higher barrier heights of TS3 and TS4 (15.1 and 118.4 kJ/mol relative to TS2), the pathway that governs the formation of the imine and HO_2 is via the five-membered-ring transition state, TS2, at atmospheric conditions.

Since the pathway proceeding via TS and TS2 is more likely at ambient conditions, the rate coefficient for this particular pathway is sensible as input for dispersion modelling. From the calculations it was apparent that the formation of TS2 is the rate determining step (r.d.s). Therefore, the rate that was calculated for the r.d.s was k_2. Since the imine is 107.9 kJ/mol more stable than the peroxy adduct, this is an exothermic reaction in equilibrium.

By using TST and RRKM, the values obtained for k_2 show a similar trend, however, the values determined using TST are an order of magnitude lower and those from RRKM are higher than the experimental value for DMA (Table 3). TST theory considers only thermal equilibrium, whereas RRKM can also account for pressure that can affect the reaction. Therefore, for this study the values obtained through RRKM are used.

3.6. *Nitrosamine photolysis: vertical excitation energies of the nitrosamines (j_5 hυ pathway)*

Nitrosamines undergo photochemical degradation in the atmosphere in the presence of solar radiation. This is due to the organic chromophore N—N=O which absorbs ultraviolet radiation around a wavelength of 365 nm and electronic excitations of n electrons to the π^* excited state resulting in N—NO bond cleavage. The photolysis of NDMA was investigated in the gas phase by Geiger and Huber (1981); Lindley et al. (1979). Tuazon et al., 1984 also determined the nitrosamine photolysis frequency relative to that of NO_2 ($J_{NDMA}/J_{NO2} = 0.53 + 0.03$), correlating to a quantum yield of 1 at 290 nm, this is in agreement to the 1.03 + 0.10 value at 363.5 nm calculated by Geiger and Huber (1981). However, owing to the very low vapour pressures of nitrosamines at atmospheric conditions, it remains challenging to perform experimental investigations. The calculated vertical excitation wavelength and oscillator strengths (0.0006–0.0011, Table 4) in this work are in agreement to the experimental findings.

The photolysis rate of nitrosamines is dependent on their spectral properties and the intensity of the solar ultraviolet radiation available. At a given latitude and longitude, the levels of solar radiation are at their maximum in the summer (~21st June), their lowest in winter (~21st December) and equal on equinox (21st March and 21st September). Hence, photolysis is the dominant gas phase removal pathway for nitrosamine during summer time. The tropo-

Table 4
Vertical electronic excitation wavelength, corresponding oscillator strength, photolysis rate, *J*, and the corresponding mean life times for the relevant *n* -> π^* transition for the three target nitrosamines predicted at TD-DFT (B3LYP/ aug-ccpTVZ) level of theory and solar actinic flux for Mongstad at mid-day for different times of the year and at 65 m stack height.

Nitrosamines	Time/ Altitude (km)	Vertical excitation wavelength (nm)	Oscillator strength	Photolysis frequency $J(s^{-1})$	$J/J(NO_2)$	Mean photolysis lifetime (τ /hr)
N-Nitroso methylamine	21st March	366.06	0.0005	2.91×10^{-3}	0.53	0.095
	21st June			4.34×10^{-3}	0.53	0.064
	21st September			2.85×10^{-3}	0.53	0.098
	21st December			4.14×10^{-4}	0.54	0.672
N-Nitroso dimethyl amine	21stMarch	358.7	0.001	6.81×10^{-3}	1.24	0.041
	21stJune	(363.5)[a]		1.02×10^{-2}	1.24	0.027
	21st September			6.66×10^{-3}	1.24	0.042
	21st December			9.64×10^{-4}	1.26	0.288
N-Nitroso monoethanolamine	21st March	367.05	0.0004	3.25×10^{-3}	0.59	0.085
	21st June			4.76×10^{-3}	0.58	0.058
	21st September			3.18×10^{-3}	0.59	0.087
	21st December			4.67×10^{-4}	0.61	0.594
	/0.5 k			$5.06 \times ^{-4}$	0.66	0.549
	/1 km			5.63×10^{-4}	0.73	0.493
	/2 km			6.64×10^{-4}	0.33	0.418

[a] Geiger and Huber (1981).

spheric ultraviolet and visible radiation model from the National Centre for Atmospheric Research (NCAR) was employed to generate solar spectral actinic flux for the latitude and longitude at which TCM is situated, at specified times of the year and at 65 m stack height (Table 4). The overlap of the simulated UV–vis spectra for the target nitrosamines and the solar actinic flux for different conditions at around 365 nm was considered. Table 4 shows the calculated photolysis frequencies and life times at the different conditions considered. The photolysis frequency is reported relative to NO_2 ($J/J(NO_2)$) using the NO_2 photolysis rate constant for the given site.

Results show that the photolysis rate constants are within the same order of magnitude for all the given nitrosamines as they all share the same organic chromophore, N—N=O. The simulated UV spectra for the three nitrosamines show a strong overlap with the solar actinic flux curves (for all the different conditions considered) around 363.5 nm, resulting in very fast photolysis rate, *J*, and consequently very short atmospheric photolysis lifetimes.

Since *J* is a function of the solar actinic flux, the obtained photolysis rate for any given nitrosamine is relatively slow in winter, therefore, they exist for longer in the atmosphere in winter. These nitrosamines have their shortest life times in the summer at the maximum available solar flux. At the two equinox conditions, the photolysis rates (and consequently the life times) are almost identical.

The primary nitrosamines (MA-NO and MEA-NO) have similar photolysis rate constants, whereas the secondary nitrosamine has a rate constant almost twice as high. Hence DMA-NO photolysis is comparatively faster resulting in a shorter lifetime.

The photolysis frequency increases with altitude (Table 4). As a consequence, the nitrosamine lifetime becomes shorter with increasing photolysis rate, as expected.

Generally, the photolysis ratio shows negligible change for any given nitrosamines, with the secondary nitrosamine having almost twice larger ratio than the two primary nitrosamines with similar values. Contrary to nitrosamines, nitramines show no absorption at wavelengths greater than 300 nm. Consequently, nitramines possess mean life times of several orders of magnitude higher than nitrosamines.

4. Atmospheric chemistry and dispersion model implementation

4.1. The ADMS 5 amine chemistry module

The atmospheric dispersion calculations were performed using the ADMS 5 Gaussian plume air dispersion model and its integrated Amine Chemistry Module (CERC, 2012d), where the user defined rate constants are provided as input parameters for each of the reaction steps within the amine chemistry module. This module can also take into account if unstable nitrosamines are formed from the emitted amine in the atmosphere. Such is the case for primary amines that form primary nitrosamines which readily isomerise to the corresponding imine. NO_x (i.e. NO and NO_2) emissions and background concentrations along with ozone background concentrations are also essential model input parameters. ADMS meteorological pre-processor data is used to determine photolysis rates on an hourly basis. The hydroxyl radical concentration is determined from the ambient ozone concentration and the photolysis rate constant for nitrogen dioxide. The emission rate for each of the emitted amine species at source is provided as input together with the amine specific rate constants. The user must also specify the parameter, *C* (Eq. 7), which is used in calculating the hourly change in the OH radical concentrations and is determined using the following relationship (CERC, 2012d):

$$C = \frac{[O_3]}{[OH]} J_{NO_2} \quad \text{(Eq.7)}$$

where

$$J_{NO_2} = 8 \times 10^{-4} \exp\left(-\frac{10}{K}\right) + 7.4 \times 10^{-6} K \quad \text{(Eq.8)}$$

Here, J_{NO_2} is the annual average photolysis rate of NO_2 (dependent on the solar radiation and latitude); ozone background concentration and OH radical concentration.

Table 5
Emitting source parameters for TCM (CERC, 2012d)

Stack height (m)	Stack diameter (m)	Plume velocity (m/s)	Emission temperature (°C)	Volume flow rate (m^3/s) at 90 °C
65	6.53	20	30	669.8

Table 6
Calculated emission rates for the individual amine species from the TCM emission data (CERC, 2012d).

Emitted species	Concentration	Emission rate (g/s)
Monomethylamine	0.1 ppmv	0.082
Dimethylamine	0.05 ppmv	0.06
Monoethanolamine	1.0 ppmv	1.623
Nitroso monoethanolamine	0.25 ppbv	4.92×10^{-4}
Nitramine	0 ppmb	
NO*x*		1.79

The input rate parameters are then used by the ADMS 5 model in determining the concentrations of the species of interest as well as the age of the primary pollutants (such as amines) at each receptor point using the standard ADMS dispersion algorithms. This process of calculating the dispersion and then the chemistry is carried out hourly. For the chemistry calculations, there needs to be the consideration of timescales. After each hourly dispersion calculation, the 'age' of the pollutants is calculated by considering the plume travel time. The reaction equations are applied over time dt to the background and then to the pollutants from the source. In addition, the dilution and entrainment calculations account for the fact that the pollutants in the plume are diluted as they travel. These last two steps are reiterated for every time step, *t*, until time equals to the pollutant age.

ADMS 5 also requires the characteristics of the emission source i.e. stack height and diameter, plume velocity, temperature, geographic location and meteorology.

4.2. Emissions, meteorology, atmospheric chemistry and tolerable and safe emission estimation for Technology Centre Mongstad

In this work, the atmospheric chemistry of DMA, MA and MEA is introduced in ADMS 5 by the rate constants presented above (Table 3). This is a significant improvement in comparison to previous studies (de Koeijer et al., 2013; Karl et al., 2011) which lacked the integration of the reaction rates into the dispersion model and relied on an inert dispersion model incorporating fixed formation yields for the degradation products.

The emission source is considered to be the absorber stack of the TCM using the same characteristics as in CERC, 2012d. The concentration of amines and amine degradation products is calculated for an area of 324 km^2 (18 km × 18 km) centred on the emitting facility for a grid resolution of 180 m × 180 m. Surface meteorological data and precipitation data from the Fesland-Bergen weather station for 2012 is obtained from the Norwegian Meteorological Institute (met.no eKlima service). The summary of parameters used in the TCM case study presented here are given in Table 5.

The dispersion model simulations for the amines of interest were performed considering a likely emission scenario taken from the CCM Project considered in CERC, 2012d (Table 6). NO_x emissions from the stack were also considered since the formation of the nitrosamines and nitramines depends on the reactions with NO and NO_2 (Table 4). The maximum estimated concentration of amine and amine degradation products in the study area was then compared to the pre-defined safety limits of the respective toxic compounds. The maximum long term average concentrations of the target amines and their corresponding NS and NA are listed in Table 7. The results are in annual average values which are used to compare with the guideline values.

In addition to the chemical transport modelling study, an Inert Dispersion Model (IDM) calculation was also performed in ADMS 5 for comparison. Fixed formation yields from experimental studies (Nielsen et al., 2011b) were applied to the IDM results to calculate the NS and NA concentrations. This modelling is referred to as the Inert Dispersion Model - Fixed Formation Yields (IDM-FFY) in this paper. These results are also shown in Table 7.

Table 7
Maximum long-term average concentrations of amines, nitrosamines and nitramines for the case scenario modelled along with the percentage transformation of the parent amine into NS and NA.

Species	Concentration ($ng\,m^{-3}$)		% Transformation of the amine to NS + NA
Monomethylamine	4.33	(4.33)	0.004
N-Nitrosomethylamine	0		
Methylnitramine	1.73×10^{-4}		
Dimethylamine	3.80	(3.81)	0.14
N-Nitroso dimethylamine	2.68×10^{-3}		
Dimethylnitramine	2.48×10^{-3}		
Monoethanolamine	1.02×10^{2}	(1.03×10^{2})	0.03
N-Nitromonoethanolamine	1.92×10^{-2}		
Ethanolnitramine	1.60×10^{-2}		
N-Nitroso dimethylamine	2.88×10^{-2}	(3.12×10^{-2})	
Nitramine	2.30×10^{-3}		
Total NS and NA	0.072		0.174

N.B Concentrations shown in brackets are from the Inert Dispersion modelling (IDM) where chemistry is not considered.

For all amines, results show that the highest concentrations of the emitted species are found within 2–3 km of the emission source owing to the dispersive effect of the atmosphere (Fig. 7). This also causes the concentrations to decrease with increasing distance from the PCCC facility. From Table 7 it can been be seen that the nitrosamines and nitramines constitute less than a percentage of the amine concentration. Table 7 shows the maximum long term calculated average concentrations for the sum of resulting NA and NS modelled for 2012 is just over 0.07 ng/m^3, which is well below the critical concentration of 0.3 ng/m^3 (Knudsen et al., 2009) for nitrosamine in the air. The calculated value is 2.2 times lower than 0.16 ng/m^3 which was calculated before (CERC, 2012d). The reason for the difference is mainly due to the use of less accurate rate constants from the literature where available and assumed rate constants for those that were not available. Therefore, this study provides more accurate results based on rate constants that were established computationally through a rigorous analysis.

Since the long term simulations considered a period of a whole year, short term average concentrations for MEA and its corresponding nitrosamines and nitramines for a single day were also calculated at the same emission rates (Fig. 7a–c). The results suggest that the concentration of the gas phase amine rises initially but then reduces monotonically and exponentially, demonstrating that the loss-only process is influenced by the amine species. The concentration of nitrosamine grows sufficiently as the amine concentration increases, but then it decreases owing to the dominance of the photo-degradation reaction. Nitramine shows a monotonic growth, though with a decreasing gradient in comparison to the nitrosamine. As the rate constant of the nitrosamine is lower than that of the nitramine, its monotonic growth is comparatively slower.

In contrast to the above results, the amine concentrations from the inert dispersion model implemented in ADMS 5 are a factor of four, three and 100 times higher for MA, DMA and MEA respectively (Table 7). Thus, the chemical transport modelling predicts lower NS and NA concentrations, although these are still within the same order of magnitude. This is in accordance with the fact that dispersion processes reduce concentrations of reactive species a lot faster than chemical transformation processes. An IDM-FFY approach was

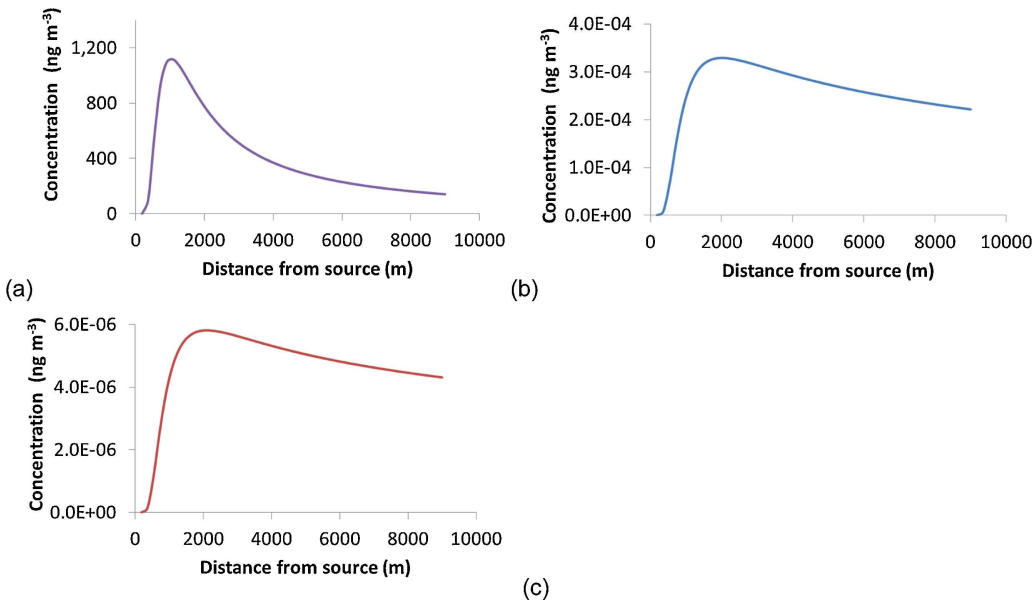

Fig. 7. Short term average concentrations (ng/m^3) against distance from source (m) for (a) MEA (b) resulting Nitrosamine (c) Nitramine, for MEA in year 2012.

also implemented to predict the maximum ambient air concentration of NS and NA (using formation yields by Nielsen et al., 2011a) which were shown to be larger by a factor of 11 relative to the chemical transport modelling.

IDM seems to always serve as a worst case upper boundary of expected concentration for the amines of interest. It only considers the amine emission without taking into account the detailed atmospheric chemistry. As a consequence, the estimated concentration of the resulting NS and NA, which pose a substantial health risk, are not evaluated accurately. It is indeed vital to obtain reliable concentrations of the resulting NA and NS within the area affected by the amine emissions around a facility to establish a realistic understanding of the human health risk they may pose.

IDM-FFY has been one of the early methods employed so as to account for experimental fixed formation yields in NA and NS concentration estimations. However, with the IDM-FFY approach, the potential risk is not spatially resolved, as the estimated concentrations of NA and NS change only in relation to conservative MEA dispersion estimates.

In conclusion, the theoretical methodology developed in this work allows to combine the estimation of reliable reaction rates derived from quantum chemistry and kinetic modelling with the chemical transport modelling. This enables to consider the entire atmospheric fate of the involved amines including their growth and decay in a given study area resulting in more accurate estimation of amine and amine degradation product concentrations over time and space. The methodology can be applied to any amines used in CO_2 capture as it is independent from experimental parameters. It is expected that this approach can also provide a valuable input in studies assessing the environmental and human health risks associated with amine emissions from PCCC facilities.

Acknowledgements

This research is funded by the Scottish Power Academic Alliance as part of the SOLVfate project carried out in collaboration with SINTEF Materials and Chemistry and supported by the CLIMIT program of the Research Council of Norway, Mitsubishi Heavy Industries and ENEL. The authors are grateful for the support of the EPSRC UK National Service for Computational Chemistry Software and the Imperial College High Performance Computing Service who supplied the computational resources. The authors also thank the Cambridge Environmental Research Consultants (CERC) for making available ADMS 5 and a specially compiled version of their Amine Chemistry module for this research. Many thanks to John Dyke and Ed Lee (University of Southampton), Gabriel da Silva (University of Melbourne), Claus Nielsen (University of Oslo) and Vladimir Mokrushin (National Institute of Standards and Technology) for helpful discussions.

Appendix A. Supplementary data

Supplementary data associated with this article can be found, in the online version, at http://dx.doi.org/10.1016/j.ijggc.2015.05.012

References

Anderson, L.G., Stephens, R.D., 1988. Kinetics of the reaction of hydroxyl radicals with 2-(dimethylamino) ethanol from 234–364 K. Int. J. Chem. Kinet. 20, 103–110.
Atkinson, R., Perry, R.A., Pitts, J.N., 1977. Rate constants for the reaction of the hydroxyl radical with methanethiol and methylamine over the temperature range 299–426 DegK. J. Phys. Chem. 66, 1578–1581.
Barker, J.R., Golden, D.M., 2003. Master equation analysis of pressure-dependent atmospheric reactions. Chem. Rev. 103, 4577–4592.
Becke, A.D., 1988. Density-functional exchange-energy approximation with correct asymptotic behavior. Phys. Rev. A 38, 3098–3100.
Bråten, H.B., Bunkan, A.J., Bache-Andreassen, L., Solimannejad, M., Nielsen, C.J., 2009. Final Report on a Theoretical Study on the Atmospheric Degradation of Selected Amines. NILU94.
Carl, S.A., Crowley, J.N., 1998. Sequential two (blue) photon absorption by NO_2 in the presence of H_2 as a source of OH in pulsed photolysis kinetic studies: rate constants for reaction of OH with CH3NH2, (CH_3) 2NH, (CH_3) 3N, and $C_2H_5NH_2$ at 295 K. J. Phys. Chem. A 102, 8131–8141.
CERC, 2012. ADMS 5 Atmospheric Dispersion Modelling System, User Guide, version 5, Cambridge, p. 412.
CERC, 2012. ADMS 5 User Guide Supplement, p. 20.
CERC, 2012. Atmospheric Chemistry Modelling – Activity 1: Gaseous Phase Chemistry Modelling (initiated by hydroxyl radical) – Executive Summary, in: Price, C., Strickland, S., Carruthers, D. (Eds.), Contract number 257,430,174: Atmospheric Chemistry Modelling. prepared for CO2Capture Mongstad Project, Statoil Petroleum SF, p. 25.
CERC, 2012. Atmospheric Chemistry Modelling Activity 1: Gaseous Phase Chemistry Modelling (initiated by hydroxyl radical), in: Price, C., Strickland, S. (Ed.), Contract number 257,430,174: Atmospheric Chemistry Modelling. prepared for CO2Capture Mongstad Project, Gassnova SF, p. 120.
da Silva, G., 2013. Formation of nitrosamines and alkyldiazohydroxides in the gas phase: the $CH_3NH + NO$ reaction revisited. Environ. Sc. Technol. 47, 7766–7772.

de Koeijer, G., Talstad, V.R., Nepstad, S., Tønnessen, D., Falk-Pedersen, O., Maree, Y., Nielsen, C., 2013. Health risk analysis for emissions to air from CO2 Technology Centre Mongstad. Int. J. Greenhouse Gas Control 18, 200–207.

Dunning, T.H., 1989. Gaussian basis sets for use in correlated molecular calculations. I. The atoms boron through neon and hydrogen. J. Chem. Phys. 90, 1007–1023.

Eyring, H., 1935. The activated complex and the absolute rate of chemical reactions. Chem. Rev. 17, 65–77.

Fernandez-Ramos, A., Miller, J.A., Klippenstein, J.S., Truhlar, D.G., 2006. Modeling the kinetics of bimolecular reactions. Chem. Rev. 106, 4518–4584.

Frisch, M.J., Trucks, G.W., Schlegel, H.B., Scuseria, G.E., Robb, M.A., Cheeseman, J.R., Scalmani, G., Barone, V., Mennucci, B., Petersson, G.A., Nakatsuji, H., Caricato, M., Li, X., Hratchian, H.P., Izmaylov, A.F., Bloino, J., Zheng, G., Sonnenberg, J.L., Hada, M., Ehara, M., Toyota, K., Fukuda, R., Hasegawa, J., Ishida, M., T. Nakajima, Y., Honda, O., Kitao, H., Nakai, T., Vreven, J. A. Montgomery, Jr., J. E. Peralta, F., Ogliaro, M., Bearpark, J. J. Heyd, E., Brothers, K. N. Kudin, V. N. Staroverov, R., Kobayashi, J., Normand, K., Raghavachari, A., Rendell, J. C. Burant, S. S. Iyengar, J., Tomasi, M., Cossi, N.R., J. M. Millam, M., Klene, J. E. Knox, J. B. Cross, V., Bakken, C., Adamo, J., Jaramillo, R., Gomperts, R. E. Stratmann, O., Yazyev, A. J. Austin, R., Cammi, C., Pomelli, J. W. Ochterski, R. L. Martin, K., Morokuma, V. G. Zakrzewski, G. A. Voth, P., Salvador, J. J. Dannenberg, S., Dapprich, A. D. Daniels, Ö., Farkas, J. B. Foresman, J. V. Ortiz, J. Cioslowski, a., Fox, D.J., 2009. Gaussian 09, Revision D.01. Gaussian, Inc., Wallingford CT.

Galano, A., Alvarez-Idaboy, J.R., 2008. Branching ratios of aliphatic amines + OH gas-phase reactions: a variational transition-state theory study. J. Chem. Theory Comput. 4, 322–327.

Galano, A., Alvarez-Idaboy, J.R., Vivier-Bunge, A., 2006. Computational quantum chemistry: a reliable tool in the understanding of gas-phase reactions. J. Chem. Edu. 83, 481.

Geiger, G., Huber, J.R., 1981. Photolysis of dimethylnitrosamine in the gas phase. Helv. Chim. Acta 64, 989–995.

Gorse, R.A., Lii, R.R., Saunders, B.B., 1977. Hydroxyl Radical Reactivity with Diethylhydroxylamine. Science 197, 1365–1367.

Harris, G.W., Pitts, J.N., 1983. Notes. Rates of reaction of hydroxyl radicals with 2-(dimethylamino) ethanol and 2-amino-2-methyl-1-propanol in the gas phase at 300. +-. 2K. Environ. Sci. Technol. 17, 50–51.

Karl, M., Brooks, S., Wright, R.F., Knuden, S., 2008. Amine Worst Case Studies. Worst case studies on amine emissions from CO2 capture plants (Task 6), Norway, pp. 14-26.

Karl, M., Dye, C., Schmidbauer, N., Wisthaler, A., Mikoviny, T., D'Anna, B., Müller, M., Borrás, E., Clemente, E., Muñoz, A., Porras, R., Ródenas, M., Vázquez, M., Brauers, T., 2012. Study of OH-initiated degradation of 2-aminoethanol. Atmos. Chem. Phys. 12, 1881–1901.

Karl, M., Wright, R.F., Berglen, T.F., Denby, B., 2011. Worst case scenario study to assess the environmental impact of amine emissions from a CO2 capture plant. Int. J. Greenhouse Gas Control 5, 439–447.

Knudsen, S., Karl, M., Randall, S., 2009. NILU Technical Report. TR 04/2009, Kjeller, Norway.

Koch, R., Krüger, H.U., Elend, M., Palm, W.U., Zetzsch, C., 1996. Rate constants for the gas-phase reaction of OH with amines: tert-butyl amine, 2,2,2-trifluoroethyl amine, and 1,4-diazabicyclo[2.2.2] octane. Int. J. Chem. Kinet. 28, 807–815.

Kootstra, F., de Boeij, P.L., Snijders, J.G., 2000. Efficient real-space approach to time-dependent density functional theory for the dielectric response of nonmetallic crystals. J. Chem. Phys. 112, 6517–6531.

Låg, M., Lindeman, B., Instanes, C., Brunborg, G., Schwarze, P., 2011. Health Effects of Amines and Derivatives Associated with CO2 Capture. The Norwegian Institute of Public Health, Oslo, Norway, pp. 45.

Lazarou, Y.G., Kambanis, K.G., Papagiannakopoulos, P., 1994. Gas-phase reactions of (CH_3) 2N Radicals with NO and NO_2. J. Phys. Chem. 98, 2110–2115.

Lepaumier, H., da Silva, E.F., Einbu, A., Grimstvedt, A., Knudsen, J.N., Zahlsen, K., Svendsen, H.F., 2011. Comparison of MEA degradation in pilot-scale with lab-scale experiments. Energy Procedia 4, 1652–1659.

Lindley, C.R.C., Calvert, J.G., Shaw, J.H., 1979. Rate studies of the reactions of the (CH_3) 2N radical with O_2, NO, and NO_2. Chem. Phys. Lett. 67, 57–62.

Magee, P., Barnes, J., 1956. The production of malignant primary hepatic tumours in the rat by feeding dimethylnitrosamine. Br. J. Cancer 10, 114.

Mokrushin, V., Bedanov, V., Tsang, W., Zachariah, M.R., Knyazev, V.D., McGivern, W.S., 2011. ChemRate, version 1.5.8;, in: Technology, N.I.o.S.a. (Ed.), Gaithersburg, MD.

Nielsen, C., D'Anna, B., Karl, M., Aursnes, M., Boreave, A., Bossi, R., Bunkan, A., Glasius, M., Hansen, A., Hallquist, M., 2011. Summary Report: Photo-oxidation of Methylamine, Dimethylamine and Trimethylamine. Climit project no. 201604 NILU OR 2/2011. ISBN 978-82-425-2357-0, NILU.

Nielsen, C.J., D'Anna, B., Dye, C., Graus, M., Karl, M., King, S., Maguto, M.M., Müller, M., Schmidbauer, N., Stenstrøm, Y., Wisthaler, A., Pedersen, S., 2011b. Atmospheric chemistry of 2-aminoethanol (MEA). Energy Procedia 4, 2245–2252.

Nielsen, C.J., Herrmann, H., Weller, C., 2012. Atmospheric chemistry and environmental impact of the use of amines in carbon capture and storage (CCS). Chem. Soc. Rev. 41, 6684–6704.

Onel, L., Blitz, M.A., Seakins, P.W., 2012. Direct determination of the rate coefficient for the reaction of oh radicals with monoethanol amine (MEA) from 296 to 510 K. J. Phys. Chem. Lett. 3, 853–856.

Onel, L., Thonger, L., Blitz, M.A., Seakins, P.W., Bunkan, A.J.C., Solimannejad, M., Nielsen, C.J., 2013. Gas-phase reactions of oh with methyl amines in the presence or absence of molecular oxygen. an experimental and theoretical study. J. Phys. Chem. A 117 (10), 736–10745.

Peng, C., Ayala, P.Y., Schlegel, H.B., Frisch, M.J., 1996. Using redundant internal coordinates to optimize equilibrium geometries and transition states. J. Comput. Chem. 17, 49–56.

Peng, C., Bernhard Schlegel, H., 1993. Combining synchronous transit and quasi-newton methods to find transition states. Isr. J. Chem. 33, 449–454.

Pople, J.A., Head-Gorden, M., Raghavachari, K., 1987. Quadratic configuration interaction – a general technique for determining electron correlation energies. J. Chem. Phys. 87, 5968–5975.

Reh, B.D., DeBord, D.G., Butler, M.A., Reid, T.M., Mueller, C., Fajen, J.M., 2000. O6-methylguanine DNA adducts associated with occupational nitrosamine exposure. Carcinogenesis 21, 29–33.

Romaniello, P., de Boeij, P.L., 2005. Time-dependent current-density-functional theory for the metallic response of solids. Phys. Rev. B 71, 155108.

Silva-Junior, M.R., Schreiber, M., Sauer, S.P., Thiel, W., 2008. Benchmarks for electronically excited states: time-dependent density functional theory and density functional theory based multireference configuration interaction. J. Chem. Phys. 129, 104103.

Stephens, P.J., Devlin, F.J., Chabalowski, C.F., Frisch, M.J., 1994. Ab initio calculation of vibrational absorption and circular dichroism spectra using density functional force fields. J. Phys. Chem. 98, 11623–11627.

Strazisar, B.R., Anderson, R.R., White, C.M., 2003. Degradation pathways for monoethanolamine in a co2capture facility. Energy Fuels 17, 1034–1039.

Tang, Y., Nielsen, C.J., 2012. A systematic theoretical study of imines formation from the atmospheric reactions of $RnNH_2$-n with O_2 and NO_2 ($R = CH_3$ and CH_3CH_2; $n = 1$ and 2). Atmos. Environ. 55, 185–189.

Thermopedia™, 2014. A-to-Z Guide to Thermodynamics, Heat & Mass Transfer, and Fluids Engineering.

Tian, W., Wang, W., Zhang, Y., Wang, W., 2009. Direct dynamics study on the mechanism and the kinetics of the reaction of CH3NH2 with OH. Int. J. Quantum Chem. 109, 1566–1575.

Tuazon, E.C., Atkinson, R., Aschmann, S.M., Arey, J., 1994. Kinetics and products of the gas-phase reactions of O_3 with amines and related compounds. Res. Chem. Intermed. 20, 303–320.

Tuazon, E.C., Carter, W.P.L., Atkinson, R., Winer, A.M., Pitts, J.N., 1984. Atmospheric reactions of n-nitrosodimethylamine and dimethylnitramine. Environ. Sci. Technol. 18, 49–54.

Wigner, E., 1932. On the quantum correction for thermodynamic equilibrium. Phys. Rev. 40, 749.

Xie, H.-B., Li, C., He, N., Wang, C., Zhang, S., Chen, J., 2014. Atmospheric chemical reactions of monoethanolamine initiated by oh radical: mechanistic and kinetic study. Environ. Sci. Technol. 48, 1700–1706.

Zhao, Y., Truhlar, D.G., 2008. Density functionals with broad applicability in chemistry. Acc. Chem. Res. 41, 157–167.

Zheng, J., Zhao, Y., Truhlar, D.G., 2009. The DBH24/08 database and its use to assess electronic structure model chemistries for chemical reaction barrier heights. J. Chem. Theory Comput. 5, 808–821.